The investigation of optical and photocatalytic properties in $Dy_2M_2O_7$ (M= Hf, Zr and Ce)

H. Zaari[a], K. Ouassoul[a], F. Mezzat[a], F. Elyahyaoui[a,*], A. El Kenz[a] and A. Benyoussef[b]

[a]*Laboratoire de Matière Condensée et Sciences Interdisciplinaires Unité de Recherche Labellisée CNRST, URL-CNRST-17, Faculté des Sciences, Mohammed V University of Rabat Morocco.*

[b]*Hassan II Academy of Science and Technology, Rabat 10000, Morocco.*

Received 20 March 2022; accepted 14 June 2022

This paper aims to present a group of compounds $Dy_2M_2O_7$ (with M = Hf, Ce and Zr) which could be an alternative having the same function as TiO_2. Based on our studies and those reported in the literature, we will discuss in detail the roles and the functional mechanism of the catalysts. The results show that $Zr_2Dy_2O_7$ is the best candidate to be a photo-catalyst: it has a band gap close to 2.2 eV, and a good absorption in visible range compared to the other compounds having absorption in UV. The quantum efficiency of $Zr_2Dy_2O_7$ reaches up to 3%, and the conduction and valence band limits are localized in a potential redox zone. Doping with Cerium gives another energy level, which allows having other optical transitions and improving the absorption and reaching the quantum efficiency to 4% in a visible range.

Keywords: DFT; photocatalysis; optical properties; quantum efficiency; potential redox.

DOI: https://doi.org/10.31349/RevMexFis.69.010501

1. Introduction

Guided by the growing energy needs, greenhouse effect and crisis of the fossil fuel resources, the search for renewable energy has become an important part of research interest [1,2]. The hydrogen energy is widely considered as one of these potential energy vectors [3,4]. Accordingly, the production of hydrogen using sunlight is a promising approach toward economical, environmentally friendly energy [5-7]. Consequently, the photo-catalytic water splitting is attracting considerable interest. The photo-catalysis process is based on the activation of a semiconductor by the sunlight, thus, an electron-positron pair is created and the photocatalyst goes into an excited state. Afterwards, the generated electron-hole pair moves to the surface of the solid. At the interface of solid and water, transported electrons and holes reduce and oxidize the adsorbed matter.

To determine the role of crystal structure on photocatalytic activity, a variety of materials with different crystal structures need to be tested. The following materials are identified as photocatalysts and active materials: $SrTiO_3$, $EuTiO_3$, $KTaO_3$, $NaTaO_3$ $Sr_2M_2O_7$ (M= Ta, Nb), $RbNdTa_2O_7$ and $La_2Ti_2O_7$ [8-10]. Rare earth-based materials are known for their use in the field of high and low temperature fuel cells, gas storage/separation, heterogeneous photo-catalysis, wastewater treatment, fluorescence and photoelectrochemical water. A different example of these materials could be cited as $La_2Zr_2O_7$, known as a semiconductor, with a band gap of 3.82 eV [11], its optical and electronic properties are modified using Ce doping at Zr site, new transitions appeared in the absorption spectra for 3.4% Ce doped $La_2Zr_2O_7$ [12]. The modified system shows an interesting behavior in its thermal conductivity, which increases as a function of temperature compared to the pure $La_2Zr_2O_7$. In addition, the effect of each concentration of Ce is studied showing that 3.4% of Ce provides the lowest thermal conductivity, the last one attributed to the high concentration of point defects affecting the phonon scattering [12].

Experimental and theoretical study of $Sm_2Zr_2O_7$ and $Dy_2Zr_2O_7$ has been done [13] to show the effect of Dy doped $Sm_2Zr_2O_7$ on the band gap and ionic conductivity. The system has a tunable band gap as function of Dy content, then its potential is explored as photo-catalyst. The synthesis by a different procedure of $Dy_2Ce_2O_7$ and $Dy_2Zr_2O_7$ reported in Refs. [14-17] show a good thermal stability during this process obtaining a pure phase of $Dy_2Ce_2O_7$ at 1500°C.

In the present study, we chose $Dy_2M_2O_7$ (M = Zr, Hf, Ce) systems as photo-catalysts for water splitting and we discuss the relationship between the photocatalytic activities and the electronic properties (band gap). Using ab-initio calculations, geometrical structure, electronic band structure and optical properties of pure $Dy_2M_2O_7$ will be calculated for (M=Hf, Ce, Zr).

There are a few details for $Dy_2M_2O_7$, so we aim to study all of the three systems and look for points of difference and resemblance based on the comparison of the electronic and optical properties.

Our study is based on DFT calculation, in the Kohn-Sham (KS) formulation, where exchange-correlation effect has been approximated, then the results depend on the chosen approximation (LDA, GGA) [18,19]. The problem appears when we get an underestimation of the KS band gap compared to whereas the experimental ones. In fact, the KS band gap is the difference in the eigenvalues of the conduction-band minimum and the valence-band maximum, the experimental band-gap is the difference between the ionization potential and the electron affinity [20]. To solve this problem many approximations have been proposed, such as GGA+U

and the modified Becke-Johnson potential (mBJ) [21]. The contribution of these approximations was well discussed, and it was noted that the correction depends on the nature material, however, generally, the mBJ correction reproduces a good value in band gap. For this reason, we have used GGA+ mBJ potential including spin-orbit coupling in our calculation. In addition, GGA+U localized the f and d states by applying the exact value of U, in our case we estimated to have the exact values for the valence band limit and the conduction band limit which further justifies our choice of mBJ approach. These values will be used to confirm the photo catalytic application of our materials.

2. Computational details

In order to describe the electronic and optical properties of pure $Dy_2M_2O_7$ (M=Hf, Ce and Zr), we used the full potential linearized augmented plane wave (FP-LAPW) method implemented in the WIEN2K code [23], within the framework of density functional theory (DFT), by treating the exchange and correlation in the level of the GGA-Perdew-Burke-Ernzerhof (GGA-PBE) approximation [24]. The basic functions, the electron densities and the potential were investigated in self-consistent manner. These quantities are developed by dividing the unit cell into non-overlapping atomic spheres, where a linear combination of radial functions times spherical harmonics is used with a cut-off parameter $l_{\max} = 10$. Moreover, we consider an interstitial region where a plane wave expansion is used with a cut-off parameter RMT*$K_{\max} = 9$, (RMT is the smallest muffin-tin radius in the unit cell and $K_{\max}$ is the magnitude of the largest K wave vector). The muffin-tin sphere radii used in the calculations are (2.37, 2.08, 1.88, a.u) for Dy, Zr, O respectively, (2.35, 2.09, 1.8) for Dy, Hf and O respectively, and (2.25, 2.32, 1.84) for Dy, Ce and O respectively. The results are obtained with an energy convergence criterion of 10^{-4} Ry. We used a (10*10*3) grid with 50 special points for sampling [25], corresponding to 400 k-points in the irreducible Brillouin zone for $Dy_2Ce_2O_7$, and (7*7*7) grid with 172 special points corresponding for both $Dy_2Hf_2O_7$ and $Dy_2Zr_2O_7$. The spin-orbit effect is also taken into calculation and TB-mBJ potential to correct the band gap value.

- The valence and conduction band edges were computed by the following equation:

$$E^0_{CB} = \chi(S) - E^0 - \frac{1}{2}E_g, \tag{1}$$

$$E^0_{VB} = E^0_{CB} + E_g, \tag{2}$$

where $\chi(S)$ is the Mulliken electronegativity E_g is the band gap energy and E^0 is the scale factor relating the electrode redox level to the absolute vacuum scale (AVS) ($E^0 \sim 4.5$ eV for normal hydrogen electrode (NHE)) [26].

- Effective mass of electrons and holes for the three compounds is computed using a fit to the equation [27]:

$$E(k) = E_0 + \left(\frac{\hbar^2 k^2}{2m*}\right), \tag{3}$$

where $E(k)$ is the energy of an electron at wavevector k in that band, E_0 is a constant giving the edge of energy of that band, and $m*$ is a constant (the effective mass). We can make a fit of the band in the direction Γ and M with the parabolic equation (for 8 points) mentioned before; we derive twice to calculate the effective mass for the holes and the electrons.

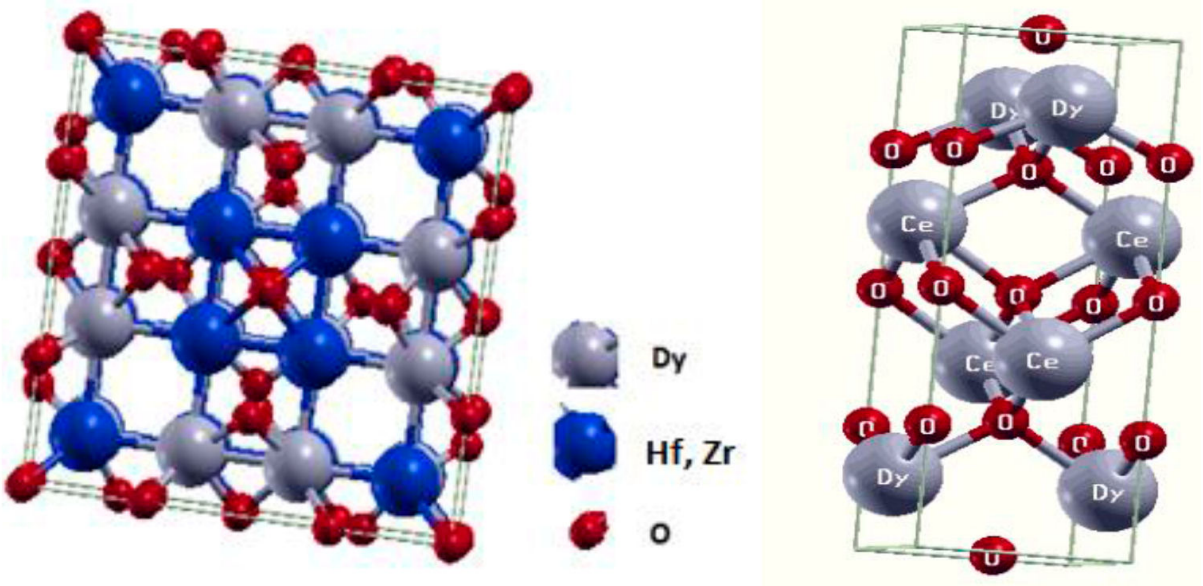

FIGURE 1. Crystal structure of $Dy_2M_2O_7$ (M=Ce, Hf and Zr) using Xcrysden code [28].

TABLE I. Structural properties $Dy_2Ce_2O_7$, $Dy_2Zr_2O_7$, $Dy_2Hf_2O_7$

	$Dy_2Hf_2O_7$	$Dy_2Zr_2O_7$	$Dy_2Ce_2O_7$
Lattice parameter (A)	10.5[29]	5.23[30]	a=3.37; c=10.9[31]
Optimized value	10.48	5.24	a=3.38; c=10.7

TABLE II. Electronic configuration and valence states of Dy, Zr, Ce and Hf atoms.

	Dy	Zr	Ce	Hf
Electronic Configuration	$4f^{10}\ 6s^2$	$4d^2\ 5s^2$	$4f^1\ 5d^1\ 6s^2$	$4f^{14}\ 5d^2\ 6s^2$
Oxidation	3	4	3,4	4
Valence	$4f^9$	$4d^0$	$4f^0$	$4f^{14}\ 5d^0$

3. Results and discussion

3.1. Electronic and optical properties

$Zr_2Dy_2O_7$ and $Dy_2Hf_2O_7$ are crystalized in a fluorite structure (Fm3m), whereas $Dy_20Ce_2O_7$ is crystallized in an orthorhombic structure (Pmma) as shown in Table I and Fig. 1.

With these structures, the nature of the atomic radius of each atom, the degree of oxidation one can predict magnetically and the electronic behavior of these compounds are computed and shown in Table II. However, a deep study on the behavior of each material will be made subsequently based on the theoretical simulation.

Based on Table II, the degree of oxidation allows us to know the occupied states, the empty states and to predict possible allowed optical transitions. To ensure the neutrality in $Dy_2Ce_2O_7$ oxidation degrees are: Ce^{4+} Dy^{3+} O^{2-}, thus all the f-Ce states, d and s states are localized in conduction band, however the f-Dy states are those which will mainly contribute to valence band for the 3 types of compounds.

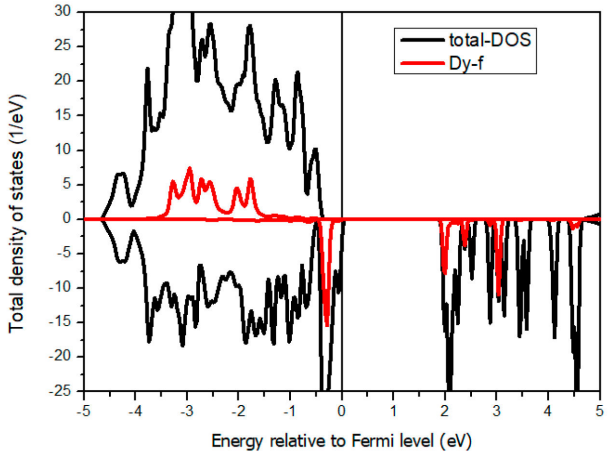

FIGURE 2. Total and partial density of states of $Dy_2Zr_2O_7$.

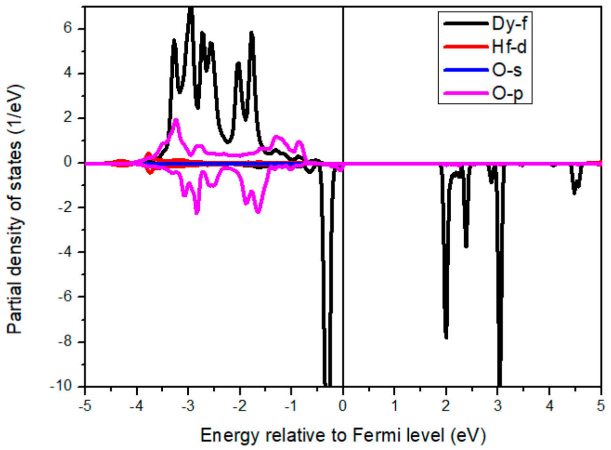

FIGURE 3. Partial density of states for $Dy_2Hf_2O_7$.

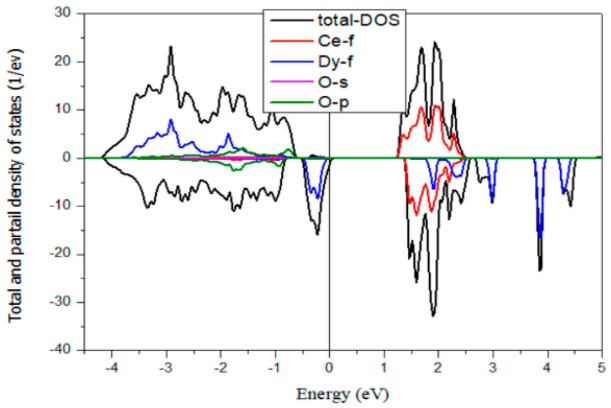

FIGURE 4. The total and partial density of states of $Dy_2Ce_2O_7$.

Based on Figs. 2, 3, 4 and Table II, the valence band is constituted by p-O and f-Dy states, while other states are localized on the conduction band. Therefore, all the allowed optical transitions are p-d and f-d: p-orbital of oxygen to d-orbital of Zr and Hf. $Dy_2Hf_2O_7$, $Dy_2Zr_2O_7$ and $Dy_2Ce_2O_7$ have an electronic band gap close to 1.89, 2.0 and 1.4 eV respectively as cited in Table III compared to other works. These values are obtained using GGA and mBJ potential including spin-orbit coupling. It is well known that standard LDA and GGA are not appropriate to compute the band gap since they give too small band gaps or even a wrong metallic behavior rather than an insulating one in some cases.

The band structure of the 3 compounds is illustrated in Figs. 5 and 6, we have a direct band gap for the 3 types,

TABLE III. Band gap of the 3 compounds compared to other works.

	$Dy_2Hf_2O_7$	$Dy_2Zr_2O_7$	$Dy_2Ce_2O_7$
Band gap (eV)	2.946[29]	3.18[30]	2.75[32]
Our results	1.89	2.0	1.4

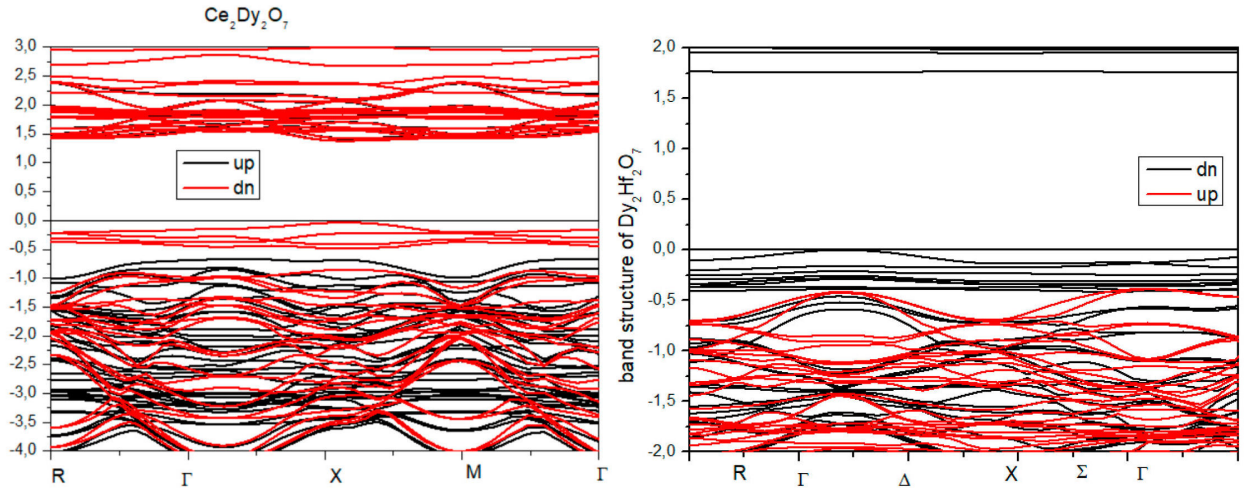

FIGURE 5. Band structure using mBJ approach of $Dy_2(Ce/Hf)_2O_7$ red (black) color present states of electrons up (dn).

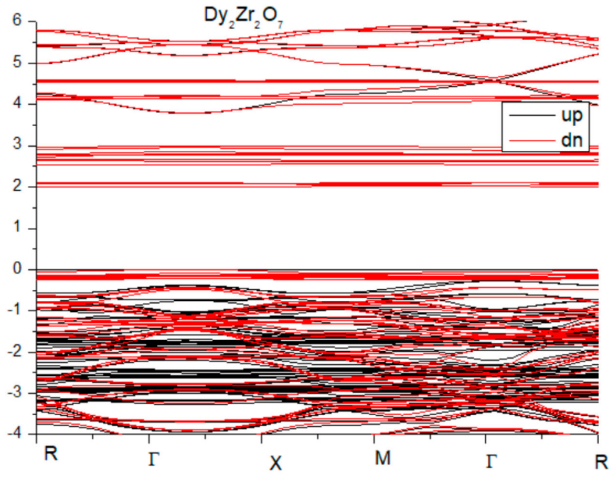

FIGURE 6. Band structure using mBJ approach of $Dy_2Zr_2O_7$ (red=dn; black=up).

with different values, the spin-orbit effect is already considered in the calculation and mBJ potential. These figures will be exploited to interpret the variation in effective mass qualitatively and quantitatively using Eq. (3).

In fact, the decisive factor for the effective mass is the curvature of the dispersion curve at the top level, as in the second derivative. Large curvatures (large second derivative = small radius of curvature) give small values of the effective mass. On the other hand, small curvatures (small derivative of a second = large radius of curvature) give large values of the effective mass.

Table IV gives the values of effective mass in Γ and M direction. We can see that these values are important in M and Γ direction for down states, for both electrons and holes, while the opposite occurs for the up states in the same directions, where the values of m^* are very low. The mobility of charge carriers in a semiconductor is inversely proportional to their effective mass (m^*). Thus, $Dy_2Hf_2O_7$ and $Dy_2Zr_2O_7$ have high mobility compared to $Dy_2Ce_2O_7$.

According to these values of effective mass, we can deduce the lifetimes of the photo-excited charge carriers and control the quantum efficiency of the photo-to-current conversion mechanism in photo-catalysis process [33].

TABLE IV. Effective mass values for Dy_2 (Ce, Hf, Zr)O_7.

	Γdirection		M direction	
	Up	dn	Up	dn
		$Dy_2Ce_2O_7$		
holes $^*m_0$	-0.92	-0.479	-0.057	-0.18
electrons (m/m$_0$)	0.07	0.27	0.057	0.238
		$Dy_2Hf_2O_7$		
holes $^*m_0$	-0.038	-0.43	-0.049	-13.97
electrons (m/m$_0$)	0.039	10.55	0,0054	infini
		$Dy_2Zr_2O_7$		
holes $^*m_0$	-0.032	-0.11	-0.043	-84.74
electrons (m/m$_0$)	0.046	0.22	0.063	0.18

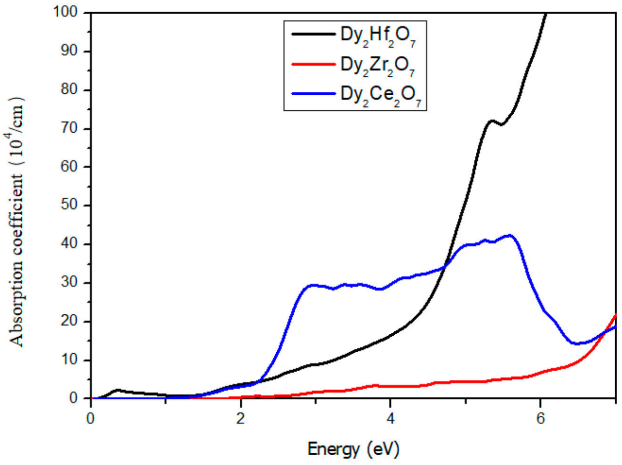

FIGURE 7. Absorption coefficient of $Dy_2M_2O_7$.

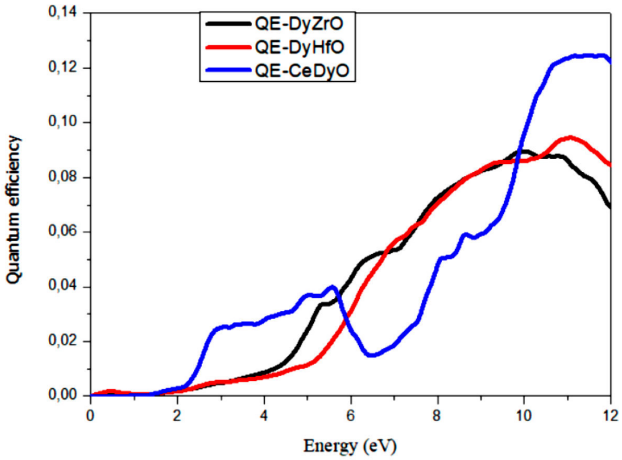

FIGURE 8. Quantum efficiency as function of energy.

3.2. Optical properties and quantum efficiency

A photocatalytic application requires a good absorption in the visible spectrum and a good optical performance. To confirm that the materials $Dy_2M_2O_7$ can be photocatalytic, we calculated the optical properties of these materials precisely: absorption coefficient and quantum efficiency. The quantum efficiency QE is an important parameter for its proportionality to the quantity of electrons/holes generated by semiconductors. It is computed using the following relation [34]:

$$QE = (1 - R)(1 - e^{\alpha t}), \tag{4}$$

where α is the absorption coefficient $\alpha(E)$ and R is the reflectivity $R(E)$. The t parameter is the thickness of the sample. Here we have used the c parameter.

According to the above relation, we have computed the absorption coefficient and quantum efficiency of all compounds; the results are displayed in Figs. 7 and 8.

There is no absorption between 0 and 2 eV in Fig. 7, except for $Dy_2Zr_2O_7$, it appears at 0.5 eV but its intensity is very weak. Also, the first peak for $Dy_2Ce_2O_7$ appears at 1.7 eV.

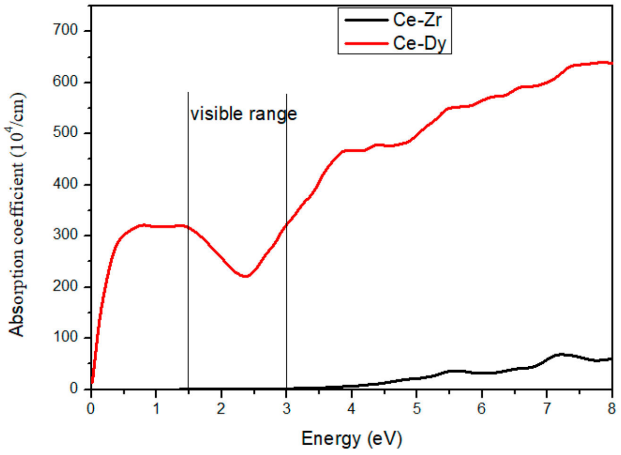

FIGURE 9. Absorption coefficient of Ce doped $Dy_2Zr_2O_7$.

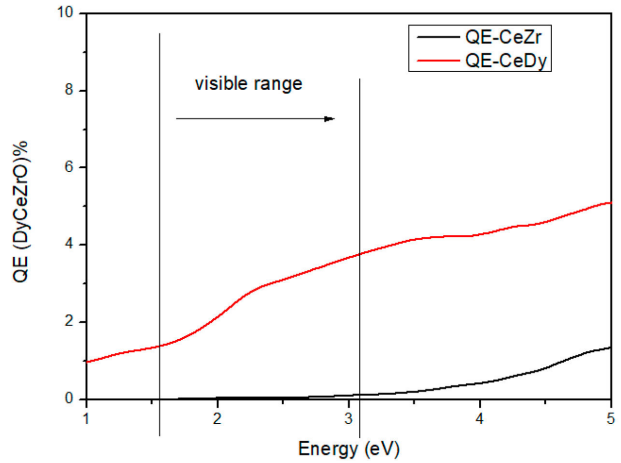

FIGURE 10. Quantum efficiency of Ce doped $Dy_2Zr_2O_7$.

In Fig. 8, we report the quantum efficiency of the 3 compound $Dy_2(Zr/Ce/Hf)_2O_7$; as we can see the quantum efficiency of $Dy_2Ce_2O_7$ reaches a maximum of 3% in visible range and it is very weak between 0 and 1.5 eV, where both compounds have lower than 1% in the visible range.

3.3. The effect of Ce Doped $Dy_2Zr_2O_7$ on the optical and electronic properties

In the last paragraph we have studied the electronic properties of Dy_2(Hf, Ce, Zr)$_2O_7$. Now, the question is, what would happen if we doped those materials and added a new state?

To get an answer for this question, we have doped Ce atoms in $Dy_2Zr_2O_7$ (25% of Ce content) in two sites:

- The first one where Ce atoms take Zr atoms' (noted CeZr) place.
- The second one where Ce atoms take Dy atoms' (noted Ce-Dy) place.

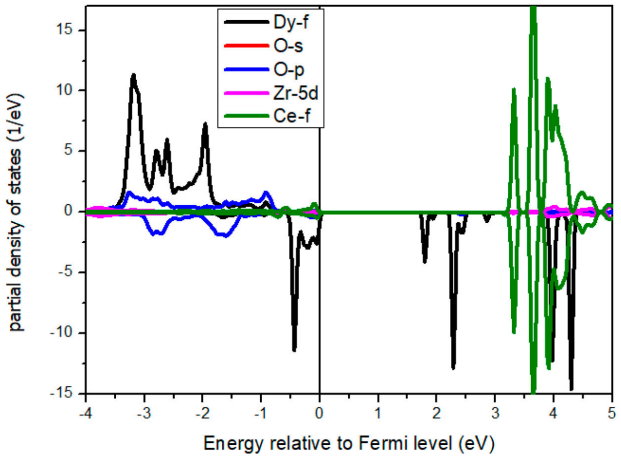

FIGURE 11. Partial density of states of $Dy_2(Ce_xZr_{1-x})_2O_7$.

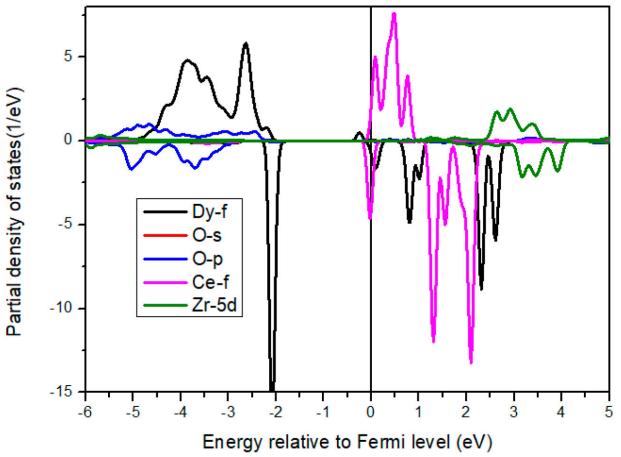

FIGURE 12. Partial density of states of $(Dy_{1-x}Ce_x)_2Zr_2O_7$.

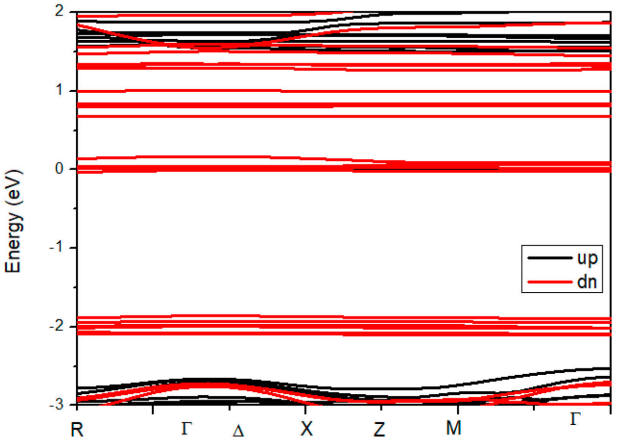

FIGURE 13. Band structure of $(DyCe)Zr_2O_7$.

We have displayed the absorption coefficient and quantum efficiency in Figs. 8 and 9.

The major difference between both cases is that the Ce doped in Zr site gives large absorption from zero and the quantum efficiency varies from 2% to 4% in visible range.

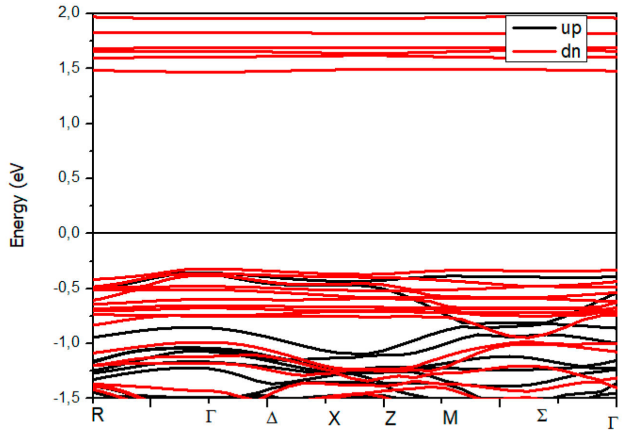

FIGURE 14. Band structure of $(DyCe)Zr_2\ O_7$.

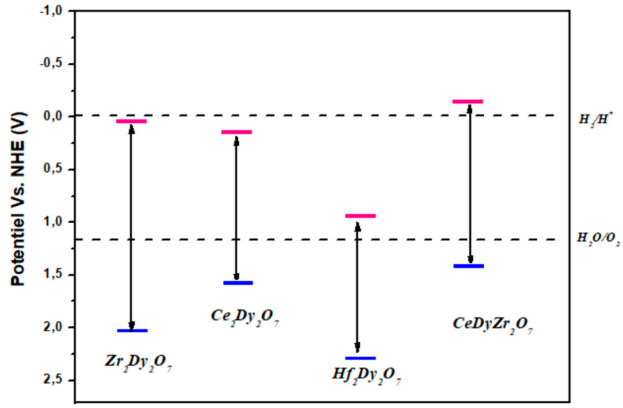

FIGURE 15. Electro-chemical potential (vs.NHE) of band edges of $Dy(Ce/Hf/Zr)O_7$.

To explain this, we look for the answer from the density of states as displayed in Figs. 10 and 11 and band structure (Figs. 12 and 13). In Zr site; f states of Cerium, are empty (Ce^{4+}: $4f^0$) localized in band conduction at 3 eV above 4f-Dy states, the gap is about 1.7 eV, and the Fermi level is near the valence band (semi-conductor p-type).

In Dy site, to ensure the neutrality of the system, we have (Dy^{3+} Ce^{3+} Zr^{4+} O^{2-}). Ce has the configuration: $4f^1$ one electron remains in valence band and it is localized near the Fermi level as shown in Figs. 13 and 14, which gives metallic behavior on the system.

3.4. Photocatalytic activity

Figure 15 presents the edges of the conduction and valence bands calculated based on absolute electronegativity, which are calculated from the ionization energy and electron affinity, and the potential H^+/H_2O and O_2/H_2O.

- For $Dy_2Ce_2O_7$ and $Dy_2Hf_2O_7$, the gap is large and exceeds the optimal value. Even the location of the bands is out of zone.

- $Dy_2Zr_2O_2$ is the best candidate to be a catalyst because

the band edges are positioned in the "redox potential" zone.

- Doping $Dy_2Zr_2O_7$ with Cerium in Zr site makes the system more accurate and promoter for photocatalytic application

4. Conclusion

To sum-up, we have used Full Potential Linearized Augmented Plan Waves to study the electronic, optical properties, quantum efficiency and photocatalytic activity for 3 different compounds ($Dy_2M_2O_7$) (M=Zr, Ce, and Hf).

The present work allows the analysis of compounds that can integrate with the family of photo catalysts through the study of 3 compounds. Through the analysis of the results obtained, it turns out that $Dy_2Zr_2O_7$ is a promising compound in photo-catalysis because of its 2.2 eV band gap. Ce doped $Dy_2Zr_2O_7$ is also a good candidate for this application.

The modification of photo-catalysts by adjusting their band structures and increasing the probability of separation of photo-generated charges leads to the progressive development of high efficiency photo-catalysts driven by visible light. To promote the efficiency of these compounds in photocatalysis, such solutions are needed: Doping or co-doping with transition metal or non-metal elements or by the realization of hetero-structures or alloy structures.

We can also think of other solutions, either a modification of the structures for band gap engineers or to put the band limits on the scale of the redox potential.

Acknowledgements

We thank P. Blaha and K. Schwarzfor the Wien2K code and the wien2k users for very useful information in the discussions.

1. L. Pérez-Lombard, J. Ortiz and C. Pout, *Energy and Buildings.* **40** (2008) 394-398.
2. M.S. Dresselhaus, and I.L. Thomas, *Nature.* **414** (2001) 332-337.
3. C. Elam, *Int. J. Hydrog. Energy* **28** (2003) 601-607.
4. M. Momirlan and T. Veziroglu, *Int. J. Hydrog. Energy*. **30** (2005) 795-802.
5. C. Byrne, G. Subramanian and S.C. Pillai, *J. Environ. Chem. Eng* **6** (2018) 3531-3555.
6. H. Ahmad, S.K. Kamarudin, L.J. Minggu and M. Kassim, *RENEW SUST ENERG REV* **43** (2015) 599-610.
7. K. Maeda and K. Domen, *J. Phys. Chem. Lett* **1** (2010) 2655-2661.
8. Ewelina Grabowska *Appl. Catal. B* **186** (2016) 97-126
9. Ryu Abe, Masanobu Higashi, Kazuhiro Sayama, Yoshimoto Abe and Hideki Sugihara *J. Phys. Chem. B* **110** (2006) 2219-2226
10. H. Zaari *et al.*, Theoretical investigation EuTiO3 in three structures; optical, electrical and magnetic properties. *Rev. Mex. Fis.* **64** (2018) 553.
11. William Duarte, Ariane Meguekam, Maggy Colas, Michel Vardelle and Sylvie Rossignol *J Mater Sci* **50** (2015) 463-475
12. S. Ramin Gul, M. Khan and Y. Zeng Bo Wu *Mater. Res. Express*, **6** (2010) 8.
13. N. Farheen *et al.*, *Inorganic Chemistry* **50** (2011) 2354-2365.
14. Zinatloo-Ajabshir S, Salehi Z and Salavati-Niasari *M. J. Clean. Prod.* **192** (2018) 678-687.
15. Farheen N. Sayed, V. Grover, K. Bhattacharyya, D. Jain, A. Arya, C. G. S. Pillai, and A. K. Tyagi *J. Phys. Chem. B* **110** (2006) 2219-2226.
16. William Duarte, Ariane Meguekam, Maggy Colas, Michel Vardelle and Sylvie Rossignol *J. Mater. Sci.* **50** (2015) 463-475.
17. A. Sachdeva, S.V. Chavan, A. Goswami, A.K. Tyagi, and P.K Pujari, *J. Solid State Chem.* **178** (2005) 2062-2066.
18. P. Hohenberg and W. Kohn, *Phys. Rev* **136** (1964) 864.
19. W. Kohn and L.J. Sham, *Phys. Rev* **140** (1965) A1133.
20. J.P. Perdew, R.G. Parr, M. Levy, and J.L. Balduz *Phys. Rev. Lett* (1982) 491691.
21. F. Tran and P. Blaha, *Phys. Rev. Lett* **102** (2009) 226401.
22. Zaari, H., El Hachimi, A. G., Benyoussef, A. and El Kenz, A *J Magn. Magn. Mater* **393** (2015) 183-187.
23. P. Blaha, K. Schwarz, G. Madsen, D. Kvasnicka, and J. Luitz, WIEN2k, augmented plane wave local orbitals program for calculating crystal properties, Vienna, Austria (2001).
24. J.P. Perdew, K. Burke, and M. Ernzerhof, *Phys. Rev. Lett*. **77** (1996) 3865-3868.
25. J. Monkhorst and J. Pack *Phys. Rev. B* **13** (1976) 5188.
26. M. Mousavi, A. Habibi-Yangjeh, and M. Abitorabi, J. Colloid Interface Sci. **480** (2016) 218-231.
27. M. A. Green, *J. Appl. Phys* **67** (1990) 2944-2954.
28. A. Kokalj and *J. Mol. Graphics Modelling* **17** (1999) 176-179.
29. X. T. Zu, N. Li, and F. Gao, *J. Appl. Phys* **104** (2008) 043517.
30. Y. Tong, Z. Yu, L. Lu, X. Yang and X. Wang *Mater. Res. Bull* **43** (2008) 2736-2741.
31. J. G. A. Ramon *et al.*, *Phys. Rev. B* **99** (2019) 214442.
32. K. Choudhary, *et al.*, *npj Comput Mater* 6 (2020) 173.
33. S. Dutta, T. Das and S. Datta, *Phys. Chem. Chem. Phys* **20** (2018) 103-111.
34. N. Baaalla, Y. Ammari, E. K. Hlil, El Kenz and A. Benyoussef, *Phys. Scr.* **95** (2020) 095104.